TU Delft

Delft University of Technology

The influence of syn-depositional compaction on clastic sediment distribution in river-dominated deltas

A modelling study

Valencia, A. A.; Storms, J. E.A.; Jagers, H. R.A.; van der Vegt, H.

DOI
10.1002/dep2.318

Publication date
2025

Document Version
Final published version

Published in
Depositional Record

Citation (APA)
Valencia, A. A., Storms, J. E. A., Jagers, H. R. A., & van der Vegt, H. (2025). The influence of syn-depositional compaction on clastic sediment distribution in river-dominated deltas: A modelling study. *Depositional Record*, *11*(2), 565-582. https://doi.org/10.1002/dep2.318

Important note
To cite this publication, please use the final published version (if applicable).
Please check the document version above.

Copyright
Other than for strictly personal use, it is not permitted to download, forward or distribute the text or part of it, without the consent of the author(s) and/or copyright holder(s), unless the work is under an open content license such as Creative Commons.

Takedown policy
Please contact us and provide details if you believe this document breaches copyrights.
We will remove access to the work immediately and investigate your claim.

This work is downloaded from Delft University of Technology.
For technical reasons the number of authors shown on this cover page is limited to a maximum of 10.

Check for updates

Received: 19 February 2024 | Revised: 5 October 2024 | Accepted: 13 October 2024

DOI: 10.1002/dep2.318

The Depositional Record Open Access
A journal of the International Association of Sedimentologists
WILEY

ORIGINAL ARTICLE

The influence of syn-depositional compaction on clastic sediment distribution in river-dominated deltas: A modelling study

A. A. Valencia[1,2] | J. E. A. Storms[1] | H. R. A. Jagers[3] | H. van der Vegt[3]

[1]Delft University of Technology, Delft, The Netherlands

[2]Universitas Indonesia, Jakarta, Indonesia

[3]Deltares, Delft, The Netherlands

Correspondence
A. A. Valencia, Delft University of Technology, Mekelweg 5, 2628 CD Delft, The Netherlands.
Email: a.a.valencia@tudelft.nl and ayunda.aulia@ui.ac.id

Funding information
Hibah Publikasi Terindeks Internasional (PUTI), Grant/Award Number: NKB-733/UN2.RST/HKP.05.00/2023

Abstract

Syn-sedimentary compaction or consolidation is an important process in deltaic environments because it affects both the local morphodynamics and hydrodynamics as well as the delta-scale accommodation space. However, the impact of syn-depositional compaction on the sediment distribution and the interdependency between different delta areas related to the sediment budget are not fully understood. This paper simulates syn-depositional compaction using improved 1D grain-size compaction formulations, integrated into hydrodynamic and morphodynamic modelling software Delft3D. The updated code is used to model sedimentation in mud-rich deltas under various compaction rate scenarios, which represents the maximum compaction rate potential of sediment that experiences the highest overburden stress in the delta. The simulated deltas are analysed by first classifying their plan-view area development into depositional elements: distributary channel, underfilled channel, delta plain, mouth bar, delta front and pro delta depositional elements. Then, sedimentation by mass, accommodation space and depositional segment metrics are calculated using the interpreted depositional elements. The results for zero compaction rate scenarios (0 mm year^{-1}) show that limited space-varying and temporal-varying accommodation is available to deposit sediment in the delta plain depositional element. Therefore, the sedimentation mainly occurs in the mouth bar depositional element. For low-mid compaction rate scenarios (0.01–1 mm year^{-1}), the additional syn-depositional accommodation space in the delta plain depositional element increases sedimentation in this area, limiting sedimentation in the mouth bar depositional element. For high compaction rate scenarios (>1 mm year^{-1}), a further increase in the accommodation space in the delta plain depositional element leads to lateral sedimentation attributed to channel relocation, where the sedimentation mainly occurs in the mouth bar depositional element. This study shows that, although considered a gradual process, syn-sedimentary compaction does impact long-term delta evolution by influencing the distribution of sedimentation in the delta.

This is an open access article under the terms of the Creative Commons Attribution License, which permits use, distribution and reproduction in any medium, provided the original work is properly cited.
© 2024 The Author(s). *The Depositional Record* published by John Wiley & Sons Ltd on behalf of International Association of Sedimentologists.

KEYWORDS
accommodation space, depositional elements, river-dominated deltas, sediment budget, sedimentation distribution, syn-depositional compaction

1 | INTRODUCTION

The interaction between sediment supply and accommodation space strongly affects the development of deltas (Muto & Steel, 1997; Colombera & Mountney, 2020). In a marine (or lacustrine) basin, accommodation space is defined as the available space between the water level and the sea floor (bathymetry), which can be regarded as static or dynamic depending on the absence or presence of relative base-level fluctuations (Koss et al., 1994; Muto & Steel, 2000, 2001; Jerolmack, 2009; Syvitski et al., 2009; Carlson et al., 2018; Dong et al., 2023). In addition to basin-scale accommodation space generation due to the change in base level, syn-depositional compaction of sediments will also contribute to local accommodation space at the depositional element (DE) scale. The local variability of accommodation interacts with the morphodynamic behaviour of the delta and, therefore, will affect the depositional patterns associated with the delta development. There is currently a lack of morphodynamic understanding related to the impact of the increased local accommodation space in the delta due to syn-depositional compaction in the clastic sediment. Recently, Valencia et al. (2023) simulated the impact of syn-depositional compaction on delta development using a constant supply of fluvial sediments (mass and grain-size distribution is not varied) and a stable relative base level. The result shows that syn-depositional compaction impacts accommodation space and distributary channel mobility, affecting depositional patterns in the simulated deltas by promoting sedimentation updip of the shoreline while limiting sediment transport downdip (Valencia et al., 2023). This result is comparable in terms of the increasing distributary channel mobility and sedimentation updip of the shoreline to general studies on the relative base-level change (Posamentier et al., 1988; Chadwick et al., 2020, 2022; Hariharan et al., 2022). This study is similar to Valencia et al. (2023), in which the accommodation space is only affected by syn-depositional compaction.

Compaction is a process of lowering bed level due to pore fluid expulsion over geological timescales ($>10^3$ years) (Greensmith & Tucker, 1986; Zoccarato et al., 2018). Consolidation is a process of lowering bed level due to pore fluid expulsion over short timescales, which can be studied in the laboratory (i.e. Bjerrum, 1967; Merckelbach & Kranenburg, 2004). This study focusses on compaction. The product of compaction is subsidence, which results in the creation of accommodation space in the basin. For example, many Holocene deltas experience accelerated subsidence due to compaction caused by excessive groundwater and/or hydrocarbon extraction (i.e. Yellow River and Vietnamese Mekong Delta) (Liu et al., 2016; Minderhoud et al., 2017; Zoccarato et al., 2018). Compaction of sediment can occur in an area with/without potential for deposition (syn-depositional and post-depositional compaction). For example, syn-depositional compaction occurs in an active delta lobe, whereas post-depositional compaction occurs in an inactive delta lobe. Both compaction types can occur interchangeably when there is a shift in the active deltaic sedimentation area due to the abandonment of an active delta lobe in preference to other locations. This study focusses on the impact of syn-depositional compaction on the active deltaic depositional area.

The active deltaic depositional area can be divided into several DEs, such as distributary channel DE, underfilled channel DE, delta plain DE, mouth bar DE, delta front DE and pro delta DE. Each DE represents a particular part of the surface extent of the depositional area. The interaction between sedimentation and erosion occurs across the boundaries of the DEs. This leads to a complex sediment dispersal system with interdependencies of DE's sediment budget. Over time, this leads to complex sedimentation patterns at the surface, which additionally impacts sediment preservation beneath the surface and generates associated heterogeneity by locally and vertically variable accumulation of sand, silt and clay. As different grain-size mixtures in the sediment compact at different rates, local syn-depositional compaction is induced, affecting the bathymetry. In turn, this affects local erosion, transport and sedimentation dynamics in DEs, illustrating a dependency loop. However, how local syn-depositional compaction impacts the distribution of deltaic sediment deposition across DEs is not yet fully understood for the following reasons: (1) compaction occurs at spatial and temporal scales that are beyond our ability to observe and measure ($>10^3$ km^2 and $>10^3$ years). (2) The preserved deltaic sediment in outcrop analogues is not complete due to erosion, leading to missing information on sedimentation and compaction history. Therefore, this dataset is difficult to use if we want to analyse the relationship between compaction and sedimentation in the delta (van der Vegt et al., 2020). Therefore, the impact of syn-depositional compaction will be addressed using a numerical simulation model.

20554877, 2025, 2, Downloaded from https://onlinelibrary.wiley.com/doi/10.1002/dep2.318 by Technical University Delft, Wiley Online Library on [28/04/2025]. See the Terms and Conditions (https://onlinelibrary.wiley.com/terms-and-conditions) on Wiley Online Library for rules of use; OA articles are governed by the applicable Creative Commons License

This paper aims to better comprehend the interdependencies of sedimentation (by mass) between DEs under the influence of syn-depositional compaction using a numerical simulation method. The focus is only on the distributary channel DE, delta plain DE and mouth bar DE because the accommodation space in these areas can be influenced by syn-depositional compaction. The delta front DE and pro delta DE are excluded from the analysis because the additional accommodation space generated by syn-depositional compaction is small compared to the overall accommodation provided by the basin water depth (Valencia et al., 2023). There are three main differences between this study and Valencia et al. (2023). First, this paper focusses on analysing the distribution of sedimentation by mass in the simulated deltas developed under the influence of compaction, in contrast to Valencia et al. (2023), which focusses on analysing morphodynamic changes in simulated deltas due to compaction. Second, an improved algorithm is employed to classify delta areas into DEs, consisting of distributary channel, underfilled channel, deltaplain, mouth bar, delta front and pro delta, compared to a more general spatial definition of delta area, such as delta top, front and pro delta used in Valencia et al. (2023). Third, the upgrade formulation for the secondary compaction that prevents accelerated reduction of sediment thickness is used, which is against the trend observed in the laboratory studies (Mesri, 2003; Merkelbach & Kranenburg, 2004).

This study is performed in several steps: (1) the formulations used to calculate compaction, previously developed by Valencia et al. (2023) are improved. (2) The improved compaction formulations are implemented into Delft3D code, which simulates river-dominated deltas where sedimentation actively occurs. (3) The simulated deltas are then analysed to understand the impact of syn-depositional compaction on the interdependencies of sedimentation (by mass) between DEs. This work builds on previous studies using Delft3D that simulate the impact of hydrodynamic forcings, supplied sediment properties and compaction on delta development (Storms et al., 2007; Edmonds & Slingerland, 2007, 2008, 2010; Edmonds et al., 2010, 2011; Geleynse et al., 2010, 2011; Nardin & Fagherazzi, 2012; Nardin et al., 2013; Caldwell & Edmonds, 2014; Hillen et al., 2014; Burpee et al., 2015; van der Vegt et al., 2020, 2016; Porcile et al., 2023; Valencia et al., 2023).

2 | METHODOLOGY FOR COMPACTING SIMULATED DELTA DEPOSITS

Several formulations have been developed to simulate compaction in unconsolidated sediments in a deltaic domain, which focus on short-timescale sedimentation ($<10^3$ years) (Winterwerp et al., 2012; Xotta et al., 2022; Zhou et al., 2016). This section describes compaction formulations for long-timescale sedimentation in a deltaic depositional environment ($>10^3$ years). Laboratory studies show thickness loss of a sediment bed initially occurs at a quicker rate after deposition, called primary compaction, followed by a slower rate, called secondary compaction (van Terzaghi, 1923; Mesri, 2003; Merckelbach & Kranenburg, 2004; Kaliakin, 2017). In this study, both compaction types will occur while deltas are evolving. Both primary and secondary compaction are therefore considered to be syn-depositional. The compaction formulations are described in the following sub-sections.

Four important assumptions are made in deriving compaction formulas that are applied in this study: (1) the sediment porosity is sufficiently high to always allow the expulsion of pore fluid. Consequently, an overpressured condition due to trapped pore fluid will not occur. (2) The pore fluid disappears after the expulsion, which does not affect the dewatering in neighbouring pores. This simplification means that the fluid flow path has no impact on long-timescale compaction ($>10^3$ years). (3) Compaction does not affect the erodibility of sediment. (4) Compaction is only applied to clastic sediment (sand and mud), as organic materials are not modelled.

2.1 | Primary compaction

Primary compaction results in a significant local thickness loss at short timescales (order of days to years) (e.g. van Asselen et al., 2009), which occurs due to grain rearrangements as pore pressures reduce (Alberts, 2005). The algorithm to calculate primary compaction is improved from Valencia et al. (2023). It is computed not only using the load imposed by overburden weight but also by self-weight, allowing for compaction of the whole model stratigraphy, including near-surface sediment, which was previously not compacted because the weight of overlying water or air was considered insignificant. The primary compaction formula is shown by Equation (1).

$$\Delta H_{\mathrm{p,t}} = C_{\mathrm{p}} \times \frac{1}{E} \times H_{t-1} \times \sigma_t \tag{1}$$

Here, the thickness loss due to primary compaction during a simulation time step ($\Delta H_{\mathrm{p,t}}$ in m) is calculated as a function of the primary compaction rate (C_{p} in m year^{-1}), Young's modulus of sediment (E in kg m^{-1}s^{-2}), the sediment thickness at the end of the previous simulation time step (H_{t-1} in m), and the load due to self-weight and overburden weight during a simulation time step (σ_{t} in Pa). The primary compaction occurs in sand and mud if

20554877, 2025, 2, Downloaded from https://onlinelibrary.wiley.com/doi/10.1002/dep2.318 by Technical University Delft, Wiley Online Library on [28/04/2025]. See the Terms and Conditions (https://onlinelibrary.wiley.com/terms-and-conditions) on Wiley Online Library for rules of use; OA articles are governed by the applicable Creative Commons License

the load is larger than that at the end of the previous simulation time step. Otherwise, secondary compaction takes place, as described in the next section.

2.2 | Secondary compaction

Secondary compaction was first explained by Taylor and Merchant (1940), who observed that compaction still occurred for conditions where there was very limited or no sedimentation occurring, yet at a much lower rate than primary compaction. This indicates that secondary compaction occurs at no/limited change in load and pore pressure (Mesri & Castro, 1987). This process is characterised by small local thickness loss per time step that occurs over a long timescale ($>10^3$ years) (Bjerrum, 1967). Secondary compaction includes processes such as plastic adjustment of sediment structure, local particle crushing and reduced absorbed water in the sediment. This compaction type only occurs in mud due to its lower permeability than sand (Zoccarato et al., 2018). The computation of local thickness loss induced by secondary compaction is based on the following approximation:

$$\Delta H_{s,t} = C_s \times H_{t-1} \times \left(\log\left(t - t_p + \Delta t\right) - \log\left(t - t_p\right)\right) \quad (2)$$

Here, the thickness loss due to secondary compaction during a simulation time step ($\Delta H_{s,t}$ in m) is a function of the secondary compaction rate (C_s in m year^{-1}), the sediment thickness at the end of the previous simulation time step (H_{t-1} in m), simulation time (t in minutes), Δt represents simulation time step (minutes) and simulation time at which primary compaction occurs (t_p in minutes). Equation 2 is an improved version from Valencia et al. (2023) because now the reference time t_p is updated each time primary compaction occurs. This prevents accelerated thickness loss as the simulation time increases, which is consistent with a previous laboratory study (Merckelbach & Kranenburg, 2004). It is important to note that the simulation time step is in hydrodynamic time, which can be converted to morphodynamic and realistic time. The different time definitions and conversion method is explained in Section 3. The derivation of the improved secondary compaction formula is explained in Text S1 (see also Figure S1).

2.3 | Subsidence

The thickness loss due to primary and secondary compaction ($\Delta H_{p,t}$ and $\Delta H_{s,t}$ in Equations 1 and 2) leads to subsidence and porosity reduction of sediment bed, shown by Equations (3) and (4).

$$H_t = H_{t-1} - \Delta H_{p|s,t} \quad (3)$$

$$\varphi_t = \varphi_{t-1} \cdot \frac{H_t}{H_{t-1}} \quad (4)$$

Here, the subsidence of sediment bed level during a simulation time step (H_t in m) is calculated by subtracting the thickness loss due to primary or secondary compaction during a simulation time step ($\Delta H_{p|s,t}$ in m) from the sediment thickness at the end of the previous simulation time step (H_{t-1} in m). The sediment porosity during a simulation time ($\emptyset_t$, dimensionless) is quantified by multiplying the sediment porosity at the end of the previous simulation time step ($\emptyset_{t-1}$, dimensionless) with the ratio of sediment thickness between two successive time steps ($\frac{H_t}{H_{t-1}}$, dimensionless). In this study, the subsidence (H_t in Equation 3) refers to compaction product, which results in subsiding bathymetry. It differs from the subsidence rate that represents the compaction rate (C_p and C_s in Equations 1 and 2). The sediment porosity ($\emptyset$) will decrease from an initial to a minimum value. The initial porosity represents the porosity of newly deposited sediment, whereas the minimum porosity represents the porosity of fully compacted sediment (Text S2).

The compaction formulations (Equations 1–4) are implemented into Delft3D code version 6.02.08.62644, which is embedded in Delft3D GUI version 4.04.01 (Deltares, 2021a). The implementation procedures can be seen in Figure S2. This Delft3D version differs from the one used by Valencia et al. (2023) because it includes a new sediment erosion formula, allowing a more stable simulation (Text S3 and Figure S3). For a detailed explanation of the processes in Delft3D, please refer to the Delft3D FLOW manual, which is available online (Deltares, 2021b).

3 | MODELLING PARAMETERS AND SCENARIOS

The updated Delft3D code is tested by simulating prograding river-dominated deltas under a stable regional relative base level. The parameters and scenarios used in the simulations are described in this section.

3.1 | Modelling parameters

The model setup consists of a discharge boundary representing a fluvial channel supplying water and sediments

20554877, 2025, 2, Downloaded from https://onlinelibrary.wiley.com/doi/10.1002/dep2.318 by Technical University Delft, Wiley Online Library on [28/04/2025]. See the Terms and Conditions (https://onlinelibrary.wiley.com/terms-and-conditions) on Wiley Online Library for rules of use; OA articles are governed by the applicable Creative Commons License

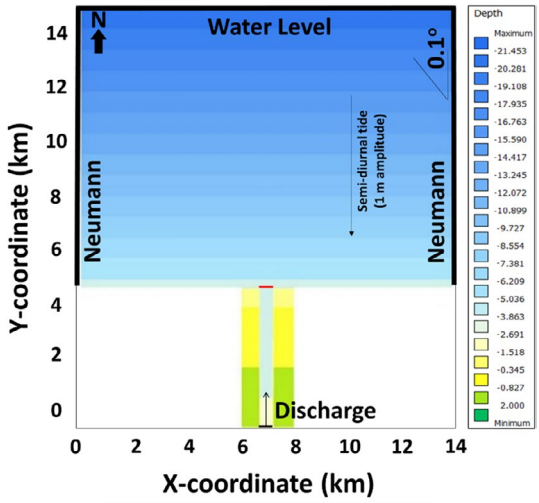

FIGURE 1 The model setup has a width and length of 14 × 15 km, consisting of a fluvial channel debouching into a sloped basin with a 0.1° gradient. The boundary condition at the channel inflow (short horizontal thin black line) is water and sediment discharge. The open boundaries in the basin (long horizontal and vertical thick black lines) are the Neumann at the west and east combined with the water level along the north boundary. The initial water depth ranges from 4 m at the delta apex (short horizontal thin red line) to 21.5 m at the basin edge.

to a sloped basin with a 0.1^0 gradient (Figure 1). A similar setup has also been used by previous modelling studies using Delft3D (Geleynse et al., 2010, 2011; van der Vegt et al., 2016, 2020; Valencia et al., 2023). The initial substrate of the model domain is sand (100 μm), which is set to fully compact by adjusting the porosity of the substrate to its minimum porosity. Sediment supplied by the fluvial channel consists of three grain-size classes (sand, 100 μm, cohesive fluvial mud, 50 and 20 μm) (Table 1). The initial substrate sand and the fluvial sand can be traced separately, even though they have identical sediment properties. The initial porosity for mud and sand was set to 80 and 40% respectively, while the minimum porosity for mud and sand was set to 5 and 25%, respectively (Revil et al., 2002; Alberts, 2005). The initial and minimum porosity of sand and mud are used to determine the initial and minimum porosity of sediment mixtures based on their proportion in the mixture (Text S2).

The model boundary representing a fluvial channel conveys a constant discharge of 1600 $m^3 s^{-1}$, with a sediment concentration of 0.15 $kg s^{-1}$ (van der Vegt et al., 2020), which allows the simulated deltas to prograde and locally aggrade during the simulation time (Text S4). As the fluvial discharge is constant over the simulation time, it is interpreted to represent a bankfull (channel forming) discharge. A low semi-diurnal tidal wave with 1 m amplitude arriving perpendicular to the initial shoreline is included in the simulations. Previous studies show that in order to simulate sedimentation similar to natural deltas, some small tidal wave activity is required to stir up the sediment deposited in the basin (van der Vegt et al., 2016, 2020). Small wind-generated waves are not included in the model setup to reduce the computation time.

The simulation time step used in this study is 0.5 min in hydrodynamic time. However, to better observe the changes in the delta development, the simulated deltas are outputted using a simulation output time step of 1 day in hydrodynamic time (Figure 2). The total simulation output time is 57 days of hydrodynamic time. This time equals 18.74 years of morphodynamic time obtained by multiplying the hydrodynamic time with the morphological scaling factor (MORFAC) of 120 as used in the model setup (Li et al., 2018). As the simulations were run using bankfull discharge, which is assumed to occur 2 days a year (Li et al., 2018), the morphodynamic time can be extended to a realistic time of 3373 years. For this study, both primary and secondary compaction operates in realistic time because: (1) the simulated deltas are formed during the flooding period (bankfull discharge) when sedimentation is active in the delta. This will activate primary compaction and, subsequently, secondary compaction if sedimentation ceases. (2) Secondary compaction occurs at a longer timescale because it has a slower compaction rate than primary compaction.

It is important to note that computed realistic time is an approximation due to the assumption that the simulation fluvial discharge is the channel-forming bankfull discharge that statistically occurs only 2 days per year and is absent during the rest of the year (363 days), which is not explicitly modelled. This means that in this model, delta dynamics are only associated with bankfull flood conditions, while in reality, sediment lower stage flow conditions will also affect the delta. In addition, bankfull discharge and its frequency in real-world systems will vary over time. Therefore, the calculated realistic time used in this study should be seen as a first-order approximation to real-world time.

3.2 | Modelling scenarios

Simulated deltas represent mud-rich deltas (85% fluvial mud and 15% fluvial sand) subjected to a range of user-defined maximum primary and secondary compaction rates (C_p and C_s in Equations 1 and 2). The primary compaction rate is the maximum expulsion rate of pore fluid due to the largest load imposed by self-weight and overburden weight, which represents compaction potential in the simulation. This parameter depends on the overall permeability of sediment mixtures, which

20554877, 2025, 2, Downloaded from https://onlinelibrary.wiley.com/doi/10.1002/dep2.318 by Technical University Delft, Wiley Online Library on [28/04/2025]. See the Terms and Conditions (https://onlinelibrary.wiley.com/terms-and-conditions) on Wiley Online Library for rules of use; OA articles are governed by the applicable Creative Commons License

TABLE 1 User-defined parameters used in all Delft3D simulations.

No	User-defined model parameter	Value	Unit
1	Grid cell dimension in x and y	50 × 50	m × m
2	Number of compacting layers	76	—
3	Initial bed thickness	4	m
4	Water discharge	1600	$m^3 s^{-1}$
5	Sediment discharge	0.15	$kg s^{-1}$
6	Total hydrodynamic time	56	day
7	Morphological scaling factor	12	—
8	Spin-up interval before morphological updating begins	720	min
9	Maximum allowed erosion rate of sediment	0.00067	$s m^{-1}$
10	Critical bed shear stress for erosion of sediment	0.18	$N m^{-2}$
11	Critical bed shear stress for deposition of sediment	1000	$N m^{-2}$
12	Grain sizes (sand and two mud fractions)	1E-04, 5E-05 and 2E-05	m
13	Specific density of sand and mud	2650	$kg m^{-3}$
14	Dry bed density of sand and mud	500 and 1600	$kg m^{-3}$
15	Settling velocity of mud fractions	0.0022 and 0.00056	$m s^{-1}$
16	Sand concentration in sediment supply	0.0225	$kg m^{-3}$
17	Mud concentration in sediment supply	0.1275	$kg m^{-3}$
18	Amplitude of semi-diurnal tide	0.02	m
19	Initial porosity of sand	0.4	—
20	Initial porosity of mud	0.8	—
21	Minimum porosity of sand	0.25	—
22	Minimum porosity of mud	0.05	—

differs in deltaic systems. The primary compaction rates are obtained from published syn-depositional compaction rates of active Holocene deltas, such as the Nile and Ganges-Brahmaputra (Stanley, 1990; Becker & Sultan, 2009; Aly et al., 2012; Gebremichael et al., 2018; Higgins et al., 2014; Saleh & Becker, 2018; Steckler et al., 2022). The primary compaction rates were set to 0–10 and 0–100 mm $year^{-1}$ in morphodynamic time for mud and sand, respectively (Table 2). Sand compacts faster because it has higher permeability than mud, resulting in the repacking of sand grains from loose to compact packing (Alberts, 2005).

As the environmental factor influencing the secondary compaction rate is still unknown (van Asselen et al., 2009), this parameter was determined by sensitivity analysis based on two criteria: (1) the secondary compaction rate should be lower than the primary compaction rate (Taylor & Merchant, 1940). (2) The determination of the secondary compaction rate is based on the modelling stability criterion. Mesri (2003) shows that the ratio secondary to primary compaction rate varies for different sediment types, for example, granular soil has a larger ratio than peat and muskeg (0.02 vs. 0.06). Different C_a/C_p values were tested, including from Mesri for shale and mudstone sediment type (0.03). The ratio values from Mesri (2003) are considered to be high, which often leads to model error because thickness reduction occurs abruptly at each simulation time. This results in a large bathymetry lowering that cannot be handled by the model. The optimum ratio value was found to be 0.0003. Therefore, the secondary compaction rate is varied from 0 to 0.003 mm $year^{-1}$ in morphodynamic time (Table 2).

Sedimentation and erosion vary in the model domain, leading to local net sedimentation rates (positive or negative) depending on local sediment accumulation rates (positive or negative). Local sediment accumulation rates cause local compaction rates. The local rates are mainly

20554877, 2025, 2, Downloaded from https://onlinelibrary.wiley.com/doi/10.1002/dep2.318 by Technical University Delft, Wiley Online Library on [28/04/2025]. See the Terms and Conditions (https://onlinelibrary.wiley.com/terms-and-conditions) on Wiley Online Library for rules of use; OA articles are governed by the applicable Creative Commons License

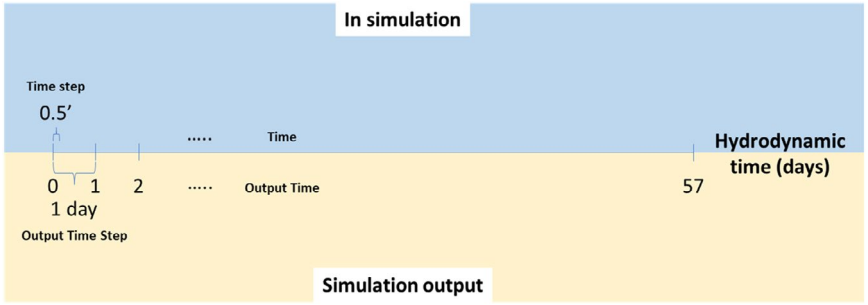

FIGURE 2 In Delt3D simulation, the calculation of delta development is conducted using a simulation time step of 0.5 minutes in hydrodynamic time. The calculation result is outputted using a simulation output time step of 1 day in hydrodynamic time. The total simulation output time is 57 days in hydrodynamic time. To better observe the changes in the delta development due to compaction over a geological timescale, the deposited sediment thickness at each simulation time is multiplied by a morphological scaling factor of 120. This leads to a total simulation time of 19 years of delta development in morphodynamic time. The timescale can be further extended by simulating the delta development over the flooding period (bankful discharge), which results in a total simulation time of 3373 years in realistic time. Simulating delta development over a flooding period means sedimentation actively occurs in the delta. This triggers the primary compaction, followed by the secondary compaction if sedimentation ceases. Therefore, primary and secondary compaction operates over the realistic time during delta development.

TABLE 2 Eight modelling scenarios (MS01–MS08) represent mud-rich deltas (85% mud and 15% sand) with varying primary and secondary compaction rates (C_p and C_s).

Run ID	C_p Mud (mm year^{-1})	C_p Sand (mm year^{-1})	C_s Mud (mm year^{-1})
MS01	0	0	0
MS02	0.01	0.1	0.000003
MS03	0.05	0.5	0.000015
MS04	0.1	1	0.00003
MS05	0.5	5	0.00015
MS06	1	10	0.0003
MS07	5	50	0.0015
MS08	10	100	0.003

slower than the primary compaction rates (Text S5), which can be considered as the compaction potential in the model. In this study, compaction rate scenarios are defined based on the primary compaction rate for mud (0–10 mm year^{-1}). Compaction rate scenarios can be converted to hydrodynamic and realistic time by considering the ratio of total simulation output time between different time definitions. For example, 1 mm year^{-1} in morphodynamic time equals 120 mm year^{-1} in hydrodynamic time (18.74 years/57/365 years is multiplied by 1 mm year^{-1}) and 0.0056 mm year^{-1} in realistic time (18.74 years/3373 years is multiplied by 1 mm year^{-1}) (Table 3).

While the simulation using compaction rate scenarios results in realistic deltas, the absolute values of compaction rate scenarios cannot be directly compared to real-world compaction measurements because: (1) they depend on assumptions used in the model (i.e. MORFAC and frequency of bankfull discharge). (2) The local compaction rates in the simulations are lower than the compaction rate scenarios (Figure S5). However, within the model domain, the zero compaction rate scenario reveals a different delta behaviour than low-mid to high compaction rate scenarios, which are analysed in the sections below. It is argued here that the relative differences between the compaction rate scenarios bear important insights that do translate to real-world deltas. Compaction rate scenarios in absolute and relative terms are shown in Table 3. Bathymetry development for all compaction rate scenarios is shown in Text S6 (Figures S6–S14).

4 | DESCRIPTION OF METRICS USED TO ANALYSE THE IMPACT OF SYN-DEPOSITIONAL COMPACTION ON SEDIMENT DISTRIBUTION IN SIMULATED DELTAS

Several metrics are developed to analyse the impact of syn-depositional compaction on the temporal evolution of simulated deltas and the distribution of sediment deposited on their surface. This allows for objective comparisons of simulated deltas' characteristics between imposed compaction rate scenarios. It is important to note that the computation of metrics is conducted for each simulation output time step starting from 15 days (in hydrodynamic time), at which the simulated deltas reach dynamic equilibrium.

20554877, 2025, 2, Downloaded from https://onlinelibrary.wiley.com/doi/10.1002/dep2.318 by Technical University Delft, Wiley Online Library on [28/04/2025]. See the Terms and Conditions (https://onlinelibrary.wiley.com/terms-and-conditions) on Wiley Online Library for rules of use; OA articles are governed by the applicable Creative Commons License

No.	Compaction rate scenarios (mm year^{-1})			
		Absolute scenarios		
	Relative scenarios	Hydrodynamic time	Morphodynamic time	Realistic time
1	Zero compaction rate	0	0	0
2	Low-mid compaction rates	1.2	0.01	5.48E-05
3		6	0.05	0.000273973
4		12	0.1	0.000547945
5		60	0.5	0.002739726
6		120	1	0.005479452
7	High compaction rates	600	5	0.02739726
8		1200	10	0.054794521

TABLE 3 Compaction rate scenarios in relative and absolute terms. The absolute term of compaction rate scenarios is defined in morphodynamic time, which can be converted into hydrodynamic and realistic time.

4.1 | Depositional elements

The first metric classifies the 2D plan-view area of simulated deltas into DEs: distributary channel DE, underfilled channel DE, delta plain DE, mouth bar DE, delta front DE and pro delta DE. These elements are identified using water depth, flow properties and deposited sediment mass (Text S7–S9 and Figures S15–S27). Over time, the accumulation of sediment in these areas will form a 3D geometry of preserved deposits called architectural elements (AE). However, the sedimentation in DEs is not equivalent to the preserved AEs due to post-depositional erosion (van der Vegt et al., 2020). The preservation of AEs is not the focus of this study.

4.2 | Distribution of sedimentation in DEs

Valencia et al. (2023) have shown that syn-depositional compaction impacts the sedimentation in various delta areas. To track the distribution of sedimentation across the delta in more detail, two metrics are used. The first metric is the percentage of sediment by mass deposited in each DE (Equation 5). This metric represents the contribution of each DE to the total sedimentation by mass in the delta. The second metric is the percentage of sediment by mass deposited in each DE for each grain-size class (Equation 6). This metric indicates the grain-size distribution of sediment deposited in DEs.

$$M_{\mathrm{DE,t}} = \frac{\mathrm{Totmass}_{\mathrm{DE,t}}}{\mathrm{Totmass}_{\mathrm{Delta,t}}} \tag{5}$$

$$M_{\mathrm{GS,DE,t}} = \frac{\mathrm{Totmass}_{\mathrm{GS,DE,t}}}{\mathrm{Totmass}_{\mathrm{Delta,t}}} \tag{6}$$

Here, the percentage of sediment by mass in DEs during a simulation output time step ($M_{\mathrm{DE,t}}$) is calculated as a ratio of total sedimentation by mass in each DE ($\mathrm{Totmass}_{\mathrm{DE,t}}$ in kg) to total sedimentation by mass in the delta ($\mathrm{Totmass}_{\mathrm{Delta,t}}$ in kg) during a simulation output time step. The percentage of sediment by mass deposited in DEs for each grain-size class during a simulation output time step ($M_{\mathrm{GS\ AE,t}}$) is quantified as the ratio of total sedimentation by mass for each grain-size class in each DE ($\mathrm{Totmass}_{\mathrm{GS,DE,t}}$ in kg) to the total sedimentation by mass for all grain-size classes in the delta ($\mathrm{Totmass}_{\mathrm{Delta,t}}$ in kg) during a simulation output time step.

To better show the influence of syn-depositional compaction on the distribution of sedimentation in DEs, the output time series of mass fractions ($M_{\mathrm{DE,t}}$ and $M_{\mathrm{GS,DE,t}}$ in Equations 5 and 6) are also collapsed into box plots. Note that the calculation of mass fractions also includes the mass eroded from the initial basin substrate. However, the contribution of eroded mass is assumed minimal as simulated deltas are actively aggrading (Figure S4).

4.3 | Accommodation

Syn-depositional compaction reduces the thickness of simulated deposited sediments, lowering the bathymetry and leading to an increase in water depth and, therefore, accommodation space (Valencia et al., 2023). The accommodation space represents the space available for potential sedimentation (Jervey, 1988; Posamentier et al., 1988). Muto and Steel (2000) further elaborates this concept by defining the accommodation space as the water depth in which the sediment can be deposited. The water depth is defined by subtracting the bathymetry from the water level. Both bathymetry and water level are measured from

20554877, 2025, 2, Downloaded from https://onlinelibrary.wiley.com/doi/10.1002/dep2.318 by Technical University Delft, Wiley Online Library on [28/04/2025]. See the Terms and Conditions (https://onlinelibrary.wiley.com/terms-and-conditions) on Wiley Online Library for rules of use; OA articles are governed by the applicable Creative Commons License

sea level. The water depth calculation is performed at each grid location for each simulation output time step.

The negative average bathymetry means the majority of DEs are above the water level or less, or no accommodation is available for sedimentation. The sediment can be above the water level if the accretion exceeds the available accommodation space in the delta plain DE. In contrast, the positive average bathymetry indicates that most DEs are below the water level and accommodation space is available for sedimentation.

4.4 | Depositional segments

Each distributary channel acts as a conduit in delivering sediments across the delta plain. Once it reaches the shoreline, the sediments are released from the channel mouths, deposited as mouth bars close to the channel mouths or travel further downdip. Therefore, the distributary channel dynamics influence the distribution of sedimentation in simulated deltas.

The change in the location of sedimentation due to distributary channel relocation is quantified using the depositional segment metric (Equation 7). Plan-view simulated deltas are divided into radial segments centring at the delta apex, consisting of central (−30° to 30°) and lateral (−90° to −30° and 30° to 90°) segments (Figure 3). The depositional segment represents the areal extent of sedimentation in the distributary channel DE and mouth bar DE, which is compared between radial segments. The main distributary channel with a well-developed mouth bar mainly influences this metric. Therefore, the mouth bar is included to amplify the contribution of the main distributary channel in the metric calculation.

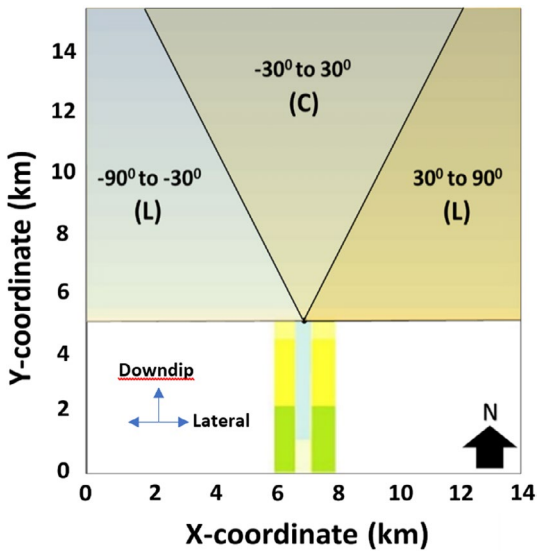

FIGURE 3 The basin area is divided into fixed radial segments centring at the delta apex: The central (−30° to 30°) and lateral (30° to 90° and −90° to −30°) segments.

$$\mathrm{Dep}_{\mathrm{segment},t} = \frac{2 * \left(A_{\mathrm{CH}} + A_{\mathrm{MB}}\right)_{C,t}}{\left(A_{\mathrm{CH}} + A_{\mathrm{MB}}\right)_{L,t}} \quad (7)$$

The depositional segment during a simulation output time step ($\mathrm{Dep}_{\mathrm{segment},t}$) is quantified as the ratio of two times the total area of distributary channel DE and mouth bar DE in the central segment ($\left(A_{\mathrm{CH}} + A_{\mathrm{MB}}\right)_{C,t}$ in m^2) to their total area in the lateral segment ($\left(A_{\mathrm{CH}} + A_{\mathrm{MB}}\right)_{L,t}$ in m^2) during a simulation output time step. Ratio values higher than two indicate that sedimentation mainly occurs in the central segment. In contrast, ratio values lower than two mean that sedimentation is primarily in the lateral segments. Note that the radial segments are fixed over the simulation output time step. Therefore, the number of distributary channels and mouth bars does not impact the metric calculation if they are located in the same segment.

5 | DELTA SIMULATION RESULTS ANALYSIS

This section reports the results and analyses of the computed metrics designed to understand the impact of compaction for various compaction scenarios. The distribution of sedimentation (by mass) in DEs will be described first, which is then linked to the accommodation and depositional segment. Only the distributary channel DE, delta plain DE and mouth bar DE are analysed and compared. The delta front DE and pro delta DE are excluded because the accommodation space in these areas is mainly influenced by the basin gradient. The underfilled channel DE is also not analysed because it has a limited contribution to the total sedimentation (by mass) in the simulated deltas.

5.1 | Distribution of sedimentation in DEs

The distribution of sedimentation in simulated deltas is analysed using the percentage of sediment by mass deposited in the system per simulation output time step, as shown in Figure 4. The result shows that the influence of syn-depositional compaction is not apparent in the temporal sedimentation trend in the distributary channel DE, delta plain DE and mouth bar DE, shown by fluctuated values of the percentage sediment by mass over the simulation output time step (Figure 4A,C,E). Temporal variability of the percentage sediment by mass can be removed

20554877, 2025, 2, Downloaded from https://onlinelibrary.wiley.com/doi/10.1002/dep2.318 by Technical University Delft, Wiley Online Library on [28/04/2025]. See the Terms and Conditions (https://onlinelibrary.wiley.com/terms-and-conditions) on Wiley Online Library for rules of use; OA articles are governed by the applicable Creative Commons License

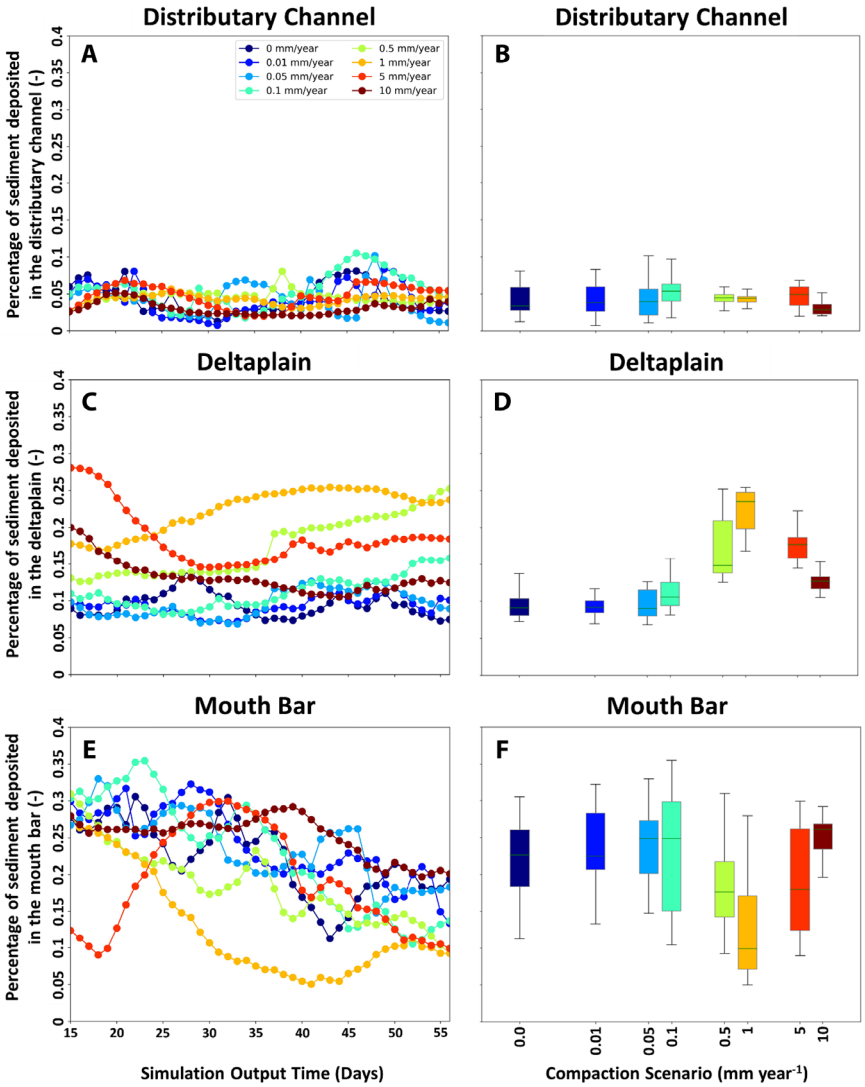

FIGURE 4 The percentage of sediment by mass deposited in the distributary channel DE, delta plain DE and mouth bar DE over the simulation output time step, starting from 15 days in hydrodynamic time (A, C and E). In the second column, the time series of the percentage sediment is collapsed by mass into box plots (B, D and F). Each box plot shows a median value (second quartile, horizontal green lines) between the first and third quartiles (interquartile range, grey boxes). The vertical black lines indicate the maximum and minimum range of data. The *x*-axis of the box plot is on a log scale. The colour indicates compaction scenarios from 0 to 10 mm year^{-1}.

by collapsing the output time series into a box plot per compaction rate scenario (Figure 4B,D,F). The distributary channel DE has a minimal response to compaction rate scenarios (Figure 4D). From zero to low-mid compaction rate scenarios (0–1 mm year^{-1}), the sedimentation (by mass) in the delta plain DE increases (Figure 4D). The opposite occurs for the mouth bar DE, where sedimentation (by mass) decreases with compaction rate scenarios (Figure 4F). In contrast, there is a negative correlation between high compaction rate scenarios (>1 mm year^{-1}) and the sedimentation (by mass) in the delta plain DE, while a positive trend is observed in the mouth bar DE (Figure 4D,F).

The grain-size distribution of sediment deposited in DEs is also compared between compaction rate scenarios using the box plots, which shows the trend better, whereas the temporal plots are in Figures S28–S30. For the distributary channel DE, the deposited mass consists of sand with lower mud content (Figure 5A,D,G). There is an increase in sand and mud sedimentation (by mass) in the delta plain DE from zero to low-mid compaction rate scenarios (0–1 mm year^{-1}) (Figure 5B,E,H). Consequently, the sedimentation (by mass) for these grain-size classes decreases in the mouth bar DE (Figure 5C,F,I). High compaction rate scenarios (>1 mm year^{-1}) show a reversed trend. For these scenarios, more compaction leads to higher sand and mud sedimentation (by mass) in the mouth bar DE. Overall, the contribution of fluvial sand to the sedimentation (by mass) in all DEs is higher than the substrate sand, which is eroded from initial basin sediment (Text S10).

The analyses of modelling results also show that the grain-size distribution of sediment deposited in DEs is not representative of the grain-size distribution of supplied sediment. For example, sand is preferentially deposited in the mouth bar DE for all compaction rate scenarios (Figure 5C). The over-representation of sand in the mouth bar DE can be attributed to the preferential sedimentation of certain grain-size classes in each DE, which is also shown in a previous study on grain-size

20554877, 2025, 2, Downloaded from https://onlinelibrary.wiley.com/doi/10.1002/dep2.318 by Technical University Delft, Wiley Online Library on [28/04/2025]. See the Terms and Conditions (https://onlinelibrary.wiley.com/terms-and-conditions) on Wiley Online Library for rules of use; OA articles are governed by the applicable Creative Commons License

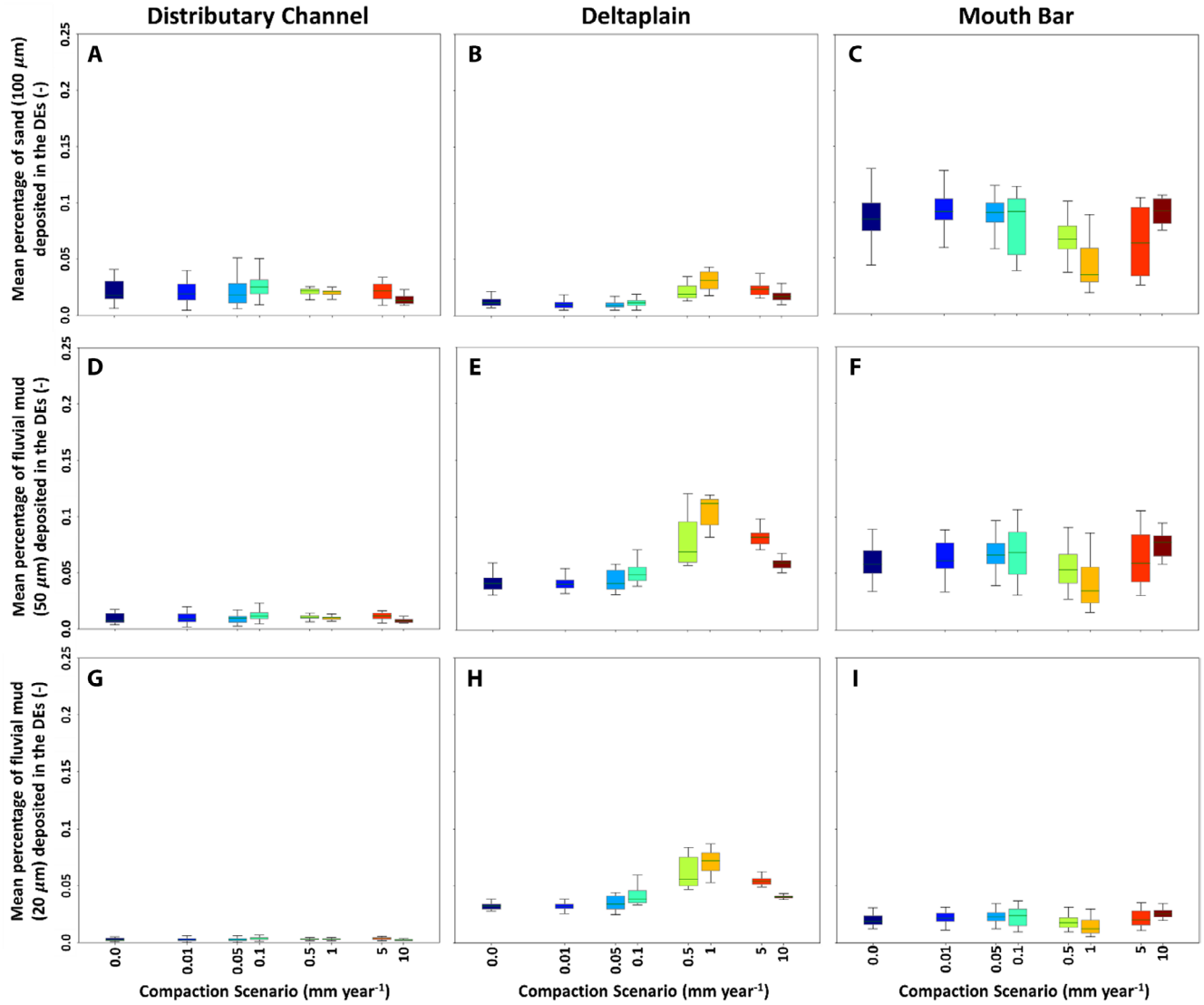

FIGURE 5 The collapsed time series of the percentage of sand and mud (by mass) deposited in distributary channel DE, delta plain DE and mouth bar DE for all compaction scenarios (A–I). Each box plot shows a median value (second quartile, horizontal green lines) between the first and third quartiles (interquartile range, grey boxes). The vertical black lines indicate the maximum and minimum range of data. The x-axis of the box plot is on a log scale. The colour indicates compaction rate scenarios. Note that sand consists of fluvial and substrate sand (Text S10).

fractionation (van der Vegt et al., 2020). Syn-depositional compaction influences this behaviour, which leads to more sedimentation of sand updip at the delta plain DE (Figure 5B). In addition, sedimentation of mud also increases in the delta plain DE than in the mouth bar DE (Figure 4E,F,H,I).

5.2 | Accommodation

Syn-depositional compaction influences the available accommodation space in the simulated deltas (Figure 6). The accommodation space increases over the simulation output time step in the distributary channel DE for all compaction rate scenarios (Figure 6A). For the same scenarios, the opposite trend occurs in the delta plain DE (Figure 6B). In contrast, compaction does not affect the temporal accommodation trend in the mouth bar DE (Figure 6C).

Comparison between compaction rate scenarios shows that the change from zero to high compaction rate scenarios (0–10 mm year^{-1}) leads to a shallowing trend in the distributary channel DE (Figure 6A). In contrast, the change from zero to low-mid compaction rate scenarios (0–1 mm year^{-1}) results in a deepening trend in the delta plain DE, whereas higher compaction rate scenarios (>1 mm year^{-1}) do not lead to greater accommodation in this area (Figure 6B). No correlation is found between the

20554877, 2025, 2, Downloaded from https://onlinelibrary.wiley.com/doi/10.1002/dep2.318 by Technical University Delft, Wiley Online Library on [28/04/2025]. See the Terms and Conditions (https://onlinelibrary.wiley.com/terms-and-conditions) on Wiley Online Library for rules of use; OA articles are governed by the applicable Creative Commons License

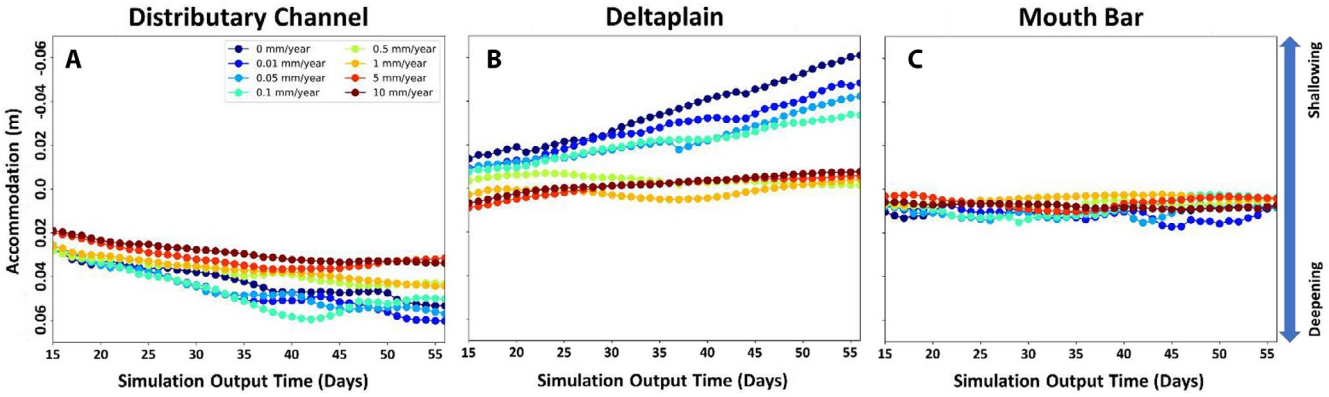

FIGURE 6 Accommodation space is represented by the relative position of bathymetry to water level in (A) the distributary channel DE, (B) delta plain DE and (C) mouth bar DE, which is averaged for each simulation output time step, starting from 15 days in hydrodynamic time. More positive accommodation means deepening, whereas more negative accommodation means shallowing. The colour indicates different compaction rate scenarios, ranging from 0 to 10 mm year^{-1}.

accommodation trend in the mouth bar DE and compaction rate scenarios (Figure 6C).

The analyses of the results also indicate that compaction rate scenarios higher than 0.5 mm year^{-1} have a comparable accommodation space, which is near zero. This happens because the accommodation space keeps being created due to syn-depositional compaction, which is then filled by sedimentation due to adequate supplied sediment. The accommodation creation updip in the distributary channel DE and delta plain DE (Figure 6A,B) influences the sedimentation (by mass) trend in the delta plain DE and mouth bar DE (Figure 4D,F). In addition, the knickpoint of 1 mm year^{-1} at which the trend change in the accommodation plot (Figure 6B,C) is consistent with the distribution of sedimentation trend (Figures 4 and 5).

5.3 | Depositional segment

The change in the main sedimentation location due to distributary channel development is analysed using the depositional segment (Figure 7). The depositional segment has increasing values during the first half of the simulation period for all compaction rate scenarios, which indicates that sedimentation increasingly occurs in the central segment (Figure 7A). The trend changes for several compaction rate scenarios (particularly >1 mm year^{-1}) during the second half of the simulation period, which shows a decrease in depositional segment values due to increased sedimentation in the lateral segments (Figure 7A).

A change in depositional segment from central to lateral can be attributed to distributary channel relocation (Figure 7B,C). The channel relocation changes the main sedimentation area to a new path (lateral), which can occur due to the creation of additional accommodation space in the delta plain DE due to syn-depositional compaction (Figure 6B). However, the mechanism for the channel relocation is not quantified in this study.

6 | INTERPRETATION OF SEDIMENT DISTRIBUTION IN DELTA SIMULATION UNDER THE INFLUENCE OF SYN-DEPOSITIONAL COMPACTION

In this section, the distribution of sedimentation (by mass) in simulated deltas experiencing syn-depositional compaction is linked to the morphodynamic response using conceptual models that show how DEs are arranged in space for zero, low-mid and high compaction rate scenarios (Figure 8). These conceptual models are derived from qualitative observation of DEs over the simulation output time step (Figures S16–S24), which is then used to draw the typical location of DEs. It is important to note that no relative base-level changes occur during the simulations.

For zero compaction rate scenario (0 mm year^{-1}), a restricted accommodation in the delta plain DE is available for sedimentation (Figure 6B). As a result, of the sediments that are captured in the delta (excluding the simulated delta front and pro delta sediments), the highest proportion of the sediment mass is deposited in the mouth bar DE, whereas a smaller proportion of sediment mass is deposited in the delta plain DE and distributary channel DE (Figure 4D,F). Sand is preferentially deposited in the mouth bar DE, leading to over-representation of this grain-size class in this area compared to other DEs (Figure 5). The depositional focus area is located in the central segment of the delta (Figure 7A,B), where the

20554877, 2025, 2, Downloaded from https://onlinelibrary.wiley.com/doi/10.1002/dep2.318 by Technical University Delft, Wiley Online Library on [28/04/2025]. See the Terms and Conditions (https://onlinelibrary.wiley.com/terms-and-conditions) on Wiley Online Library for rules of use; OA articles are governed by the applicable Creative Commons License

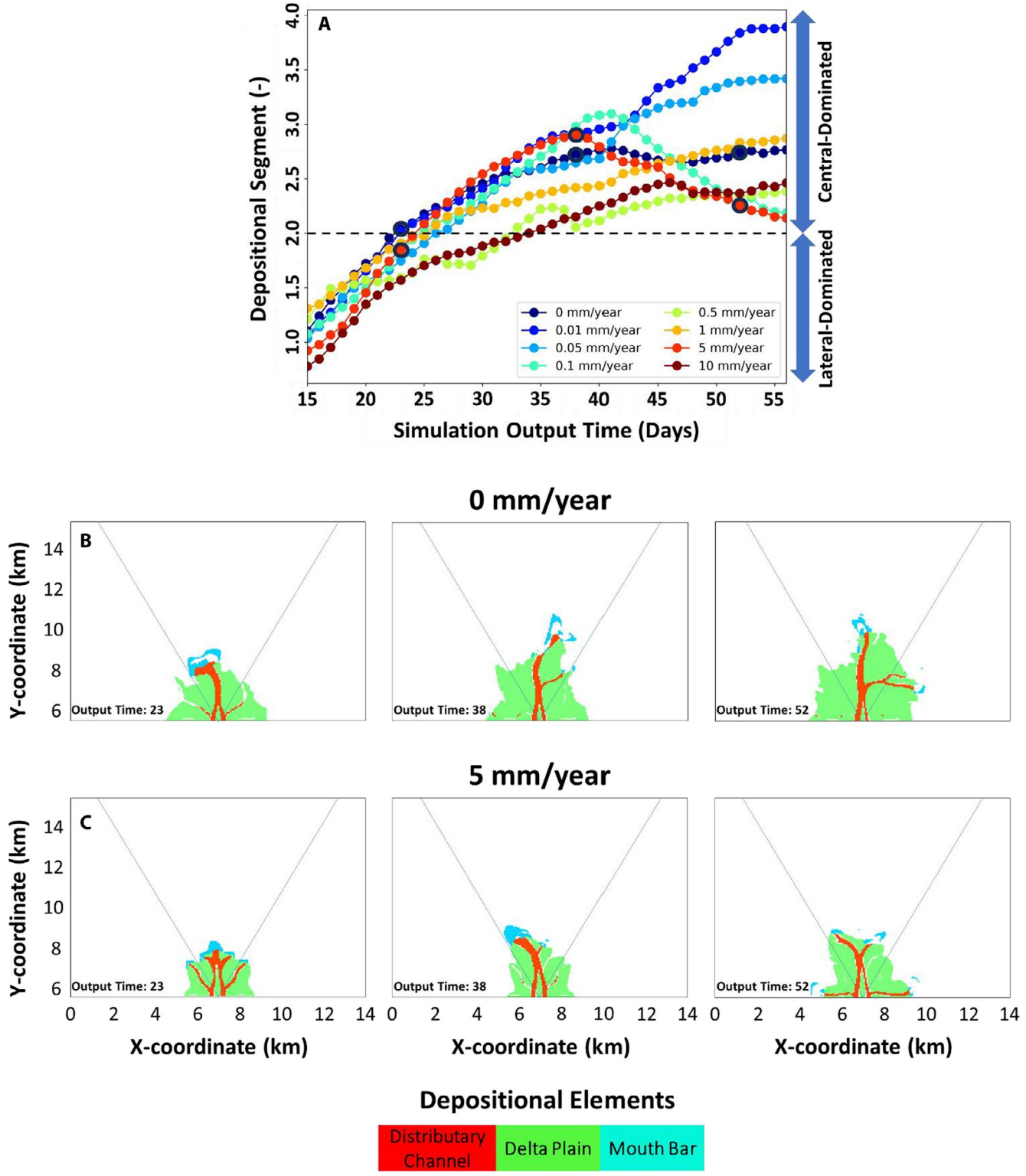

FIGURE 7 The change in the main sedimentation location due to distributary channel development is estimated using the depositional segment metric, calculated for each simulation output time step starting from 15 days in hydrodynamic time (A). The depositional segment values higher than two (marked by a black horizontal dashed line in (A) indicate that the sedimentation mainly occurs in the central segment. In contrast, sedimentation primarily occurs in the lateral segments if the depositional segment values are lower than two. The plan-view depositional elements at selected simulation output time (marked by empty black dots in (A) are shown for compaction scenarios 0 mm year^{-1} and 5 mm year^{-1} (B and C). The diagonal blue lines in (B) and (C) are boundaries between the central and lateral segments.

20554877, 2025, 2, Downloaded from https://onlinelibrary.wiley.com/doi/10.1002/dep2.318 by Technical University Delft, Wiley Online Library on [28/04/2025]. See the Terms and Conditions (https://onlinelibrary.wiley.com/terms-and-conditions) on Wiley Online Library for rules of use; OA articles are governed by the applicable Creative Commons License

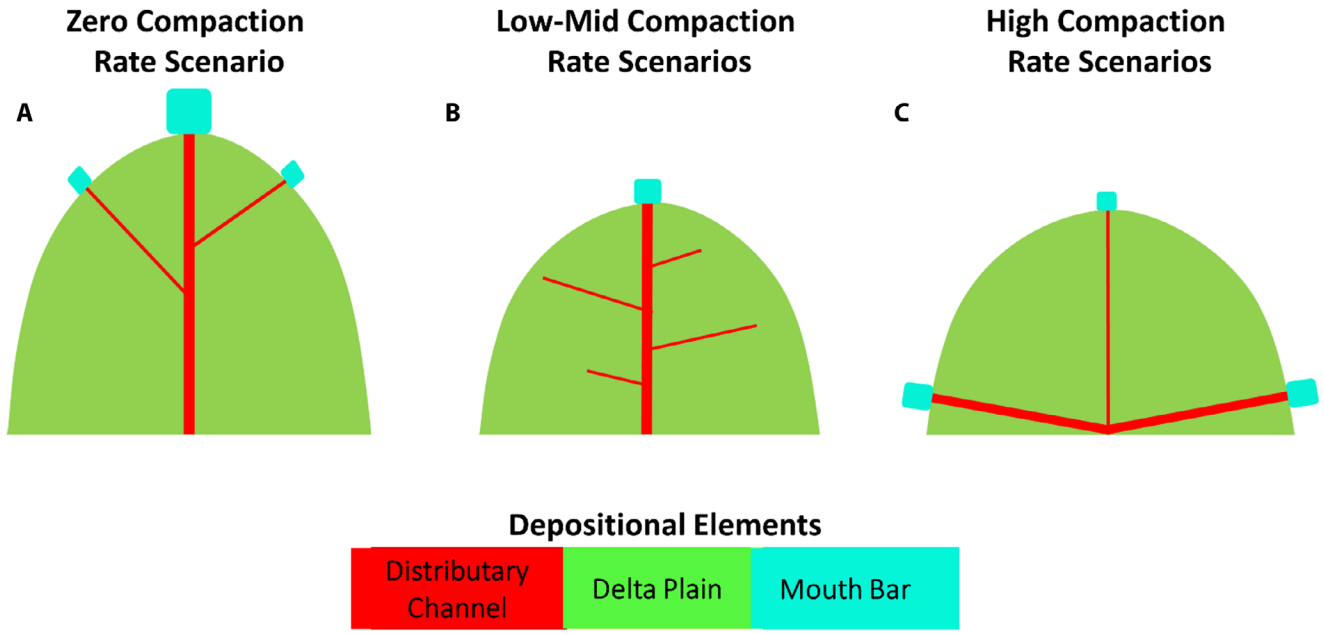

FIGURE 8 The conceptual models show depositional elements (distributary channel DE, delta plain DE and mouth bar DE) arranged in space for (A) zero, (B) low-mid and (C) high compaction rate scenarios.

distributary channel DE and mouth bar DE are mainly situated (Figure 8A). Therefore, the land building in the delta primarily occurs in this segment.

From low to mid compaction scenarios (0.01–1 mm year^{-1}), syn-depositional compaction creates additional accommodation space in the delta plain DE (Figure 6B). This leads to more sedimentation in the delta plain DE, consisting of sand and mud (Figures 4D and 5B,E,H). Consequently, less sediment for the same grain-size classes is available for the mouth bar DE (Figures 4F and 5C,F,I). The depositional focus area is more towards the lateral segments of the deltas due to the development of small distributary channels DE in these segments (Figure 8B). The small channels supply sediment to the delta plain DE to compensate for the compaction-induced additional accommodation space in this area. The highest sedimentation in the simulation occurs at compaction rate scenarios of 1 mm year^{-1} (a mid compaction scenario). This means that the highest compaction scenario does not lead to the largest sedimentation in the deltaplain, which contrasts with the findings from Nienhuis et al. (2018).

For high compaction scenarios (>1 mm year^{-1}), significant accommodation space is created in the delta plain DE (Figure 6B). Locally, this will lead to drowning when the local sediment supply is insufficient to compensate for the increase in accommodation space (Figure 6B). The depositional focus area shifts towards the lateral segments of the deltas (Figure 7A,C), where sedimentation mainly takes place in the mouth bar DE (Figure 4D,F). The shift can occur due to channel relocation (Figure 8C) in response to accommodation space creation in the lateral segments. However, the relationship between channel dynamics and compaction-induced accommodation space is not specifically analysed in this study.

7 | DISCUSSION

In the previous section, the directional shift in the depositional focus for high compaction rate scenarios is attributed to distributary channel relocation (Figure 8C), which is linked to compaction-induced accommodation space. However, previous studies also show that an upstream increase in the water level in the channel (the backwater effect) can be an important factor affecting the channel relocation (Chadwick et al., 2022; Zheng et al., 2019). The backwater occurs when the channel discharge approaches the standing body of water. The channel flow interacts with the water body at the outlet, which is, in this study, affected by the incoming tide. In general, the flow gradually adjusts its water level and velocity, which can increase the water level in the channel (Chadwick et al., 2022). To assess whether the backwater affects the channel relocation in simulated deltas, the mean water level is calculated for areas that fall in different radii from the delta apex (Text S11 and Figure S31). The results show that the water level in all areas has a small variation (up to 25 cm) over the simulation output time, suggesting that the backwater is not responsible for the channel relocation in simulated deltas.

In this study, the simulated delta plain is not vegetated, which differs from all but arctic Holocene deltas. In

20554877, 2025, 2, Downloaded from https://onlinelibrary.wiley.com/doi/10.1002/dep2.318 by Technical University Delft, Wiley Online Library on [28/04/2025]. See the Terms and Conditions (https://onlinelibrary.wiley.com/terms-and-conditions) on Wiley Online Library for rules of use; OA articles are governed by the applicable Creative Commons License

addition, contemporary deltas are influenced by human activity (Syvitski & Saito, 2007; Day & Giosan, 2008; Syvitski et al., 2009; Liu et al., 2016; Bussi et al., 2021). The simulated deltas are, therefore, best represented by natural unvegetated artic deltas, such as Greenlandic deltas. These deltas grow rapidly due to high sediment supply and sea-level fall, particularly during the spring and summer conditions, when extensive snow and ice sheets melt (Overeem et al., 2017, 2022). In addition, their location in fjords limits deltaic wave reworking and the sediment is rich in meltwater (Overeem et al., 2022; Syvitski et al., 2022). However, accurate comparison between simulated and Greenlandic deltas may be difficult because key processes that influence the development of these deltas are different. The Greenlandic deltas experience relative base-level fall due to isostatic rebound triggered by ice-sheet melt (Wake et al., 2016), whilst no relative base-level change occurs in this study. In addition, the supply sediment of Greenlandic deltas is mainly coarse-grained (Syvitski et al., 2022), which contrasts with fine-grained in this study. Therefore, the insight from this study is used to interpret real-world deltas. Syn-depositional compaction will impact the depositional nature of the Greenlandic deltas, leading to more sediment retention in the delta plain, depending on syn-depositional compaction rates and associated accommodation space created in this area. This will influence the amount of sediment (and associated nutrients) flux transported to the ocean.

van der Vegt et al. (2020) studied the distribution of preserved sediment (by mass) in simulated deltas using Delft3D. The results show that the delta plain deposits contribute to less than 5% of the total mass preserved in the deltas, which is attributed to very little sedimentation in this area. The relationship between sedimentation and sediment preservation was not specifically analysed. However, this study indicates that limited sedimentation in the previous study can occur because the processes that are responsible for capturing sedimentation in the delta plain, such as syn-depositional compaction and vegetation, are not simulated. Compaction in the delta plain area results in subsidence of the sediment bed, lowering the delta plain surface elevation and creating additional accommodation space to deposit more sediment in this area. Albernaz et al. (2020) showed that vegetation influences the number of crevasses that act as passages to transport sediment from the distributary channel to the delta plain. Coarse-grained sediment is mainly deposited within the crevasse channel, whilst fine-grained sediment is transported across the delta plain (Cazanacli & Smith, 1998), which defines the area of crevasse splays. Vegetation alters the critical bed shear stress and the roughness of the delta plain sediment, which reduces erosion by the crevasse channel. This leads to intricate crevasse channel patterns (Albernaz et al., 2020). Vegetation also reduces the flow velocity, retaining more sediment in the delta plain (Cazanacli & Smith, 1998; Nienhuis et al., 2018; Albernaz et al., 2020). Therefore, if vegetation is combined with compaction in this study, a further increase in sedimentation in the delta plain area is expected.

Understanding the link between compaction and vegetation in delta settings is important but it is not well-studied. Positive and negative feedback loops can occur due to interaction between compaction and vegetation during the growth and decay period. During the growth period, the stems and leaves increase the roughness, reducing flow velocity and promoting sedimentation (Baustian et al., 2018; Albernaz et al., 2020), which complements the compaction impact on retaining sediment due to additional accommodation space (positive feedback loop). However, a decrease in porosity of the sediment bed due to compaction also restricts root penetration to reach water and nutrients, which affects vegetation growth (negative feedback loop) (Kozlowski, 1999). During the decay period, the plant debris increases the bed level, reducing accommodation space created by compaction, which contrasts with the impact compaction has on increasing accommodation space (negative feedback loop). In addition, plant debris influences bed composition, which affects compaction (i.e. overburden stress, initial porosity and minimum porosity of sediment bed). Simulating complex interactions between compaction and vegetation in the delta would help to predict land reclamation and restoration projects and should, therefore, be a key direction of Delft3D code development in the future.

8 | CONCLUSION

A new compaction algorithm was successfully implemented into Delft3D and used to generate seaward prograding and aggrading deltas with varying compaction rate scenarios (0–10 mm year^{-1}). The simulated deltas were analysed using metrics that calculate the distribution of sedimentation by mass, accommodation space and depositional segment. Based on the analysis, it is possible to conclude:

- Syn-depositional compaction influences the location of sedimentation (by mass), driven by the change in accommodation space in DEs. This leads to interdependency of sediment budget between DEs.
- For zero compaction rate scenario (0 mm year^{-1}), no additional accommodation space is created. Therefore, the sediment quickly fills the available accommodation

20554877, 2025, 2, Downloaded from https://onlinelibrary.wiley.com/doi/10.1002/dep2.318 by Technical University Delft, Wiley Online Library on [28/04/2025]. See the Terms and Conditions (https://onlinelibrary.wiley.com/terms-and-conditions) on Wiley Online Library for rules of use; OA articles are governed by the applicable Creative Commons License

space in the delta plain DE, while the majority of sediment bypasses towards the mouth bar DE.
- For low-mid compaction rate scenarios (0.01–1 mm year^{-1}), more sedimentation (by mass) occurs in the delta plain DE due to additional accommodation created in this area, resulting in less sedimentation (by mass) in the mouth bar DE.
- For high compaction rate scenarios (>1 mm year^{-1}), extensive accommodation leads to a change in the main sedimentation area to the lateral side of the delta due to channel relocation, where the main sedimentation mainly occurs in the mouth bar DE.

ACKNOWLEDGEMENTS

We acknowledge the Hibah Publikasi Terindeks Internasional (PUTI) Q2 No. NKB-733/UN2.RST/HKP.05.00/2023 from Universitas Indonesia, which the first author receives. The authors would also like to thank Prof. Allard Willem Martinus for the insightful comments on the final draft.

CONFLICT OF INTEREST STATEMENT

The authors declare no conflicts of interest.

DATA AVAILABILITY STATEMENT

Simulation input, output and post-processed data used in this study can be accessed at: https://surfdrive.surf.nl/files/index.php/s/LHVoddfD1EmwwSI.

ORCID

A. A. Valencia https://orcid.org/0000-0002-5807-4585
J. E. A. Storms https://orcid.org/0000-0002-8902-8493
H. van der Vegt https://orcid.org/0000-0003-0506-8744

REFERENCES

Albernaz, M.B., Roelofs, L., Pierik, H.J. & Kleinhans, M.G. (2020) Natural levee evolution in vegetated fluvial-tidal environments. *Earth Surface Processes and Landforms*, 45, 3824–3841. https://doi.org/10.1002/esp.5003

Alberts, L.J.H. (2005) Initial porosity of random packing: computer simulation of grain rearrangement (Doctoral Thesis). Delft University of Technology, Delft.

Aly, M.H., Klein, A.G., Zebker, H.A. & Giardino, J.R. (2012) Land subsidence in the Nile Delta of Egypt observed by persistent scatterer interferometry. *Remote Sensing Letters*, 3, 621–630. https://doi.org/10.1080/01431161.2011.652311

Baustian, M.M., Meselhe, E., Jung, H., Sadid, K., Duke-Sylvester, S.M., Visser, J.M., Allison, M.A., Moss, L.C., Ramatchandirane, C., van Maren, D.S., Jeuken, M. & Bargu, S. (2018) Development of an Integrated Biophysical Model to represent morphological and ecological processes in a changing deltaic and coastal ecosystem. *Environmental Modelling & Software*, 109, 402–419. https://doi.org/10.1016/j.envsoft.2018.05.019

Becker, R.H. & Sultan, M. (2009) Land subsidence in the Nile Delta: inferences from radar interferometry. *The Holocene*, 19, 949–954. https://doi.org/10.1177/0959683609336558

Bjerrum, L. (1967) Engineering Geology of Norwegian Normally-Consolidated Marine Clays as Related to Settlements of Buildings. *Géotechnique*, 17, 83–118. https://doi.org/10.1680/geot.1967.17.2.83

Burpee, A.P., Slingerland, R.L., Edmonds, D.A., Parsons, D., Best, J., Cederberg, J., McGuffin, A., Caldwell, R., Nijhuis, A. & Royce, J. (2015) Grain-Size Controls On the Morphology and Internal Geometry of River-Dominated Deltas. *Journal of Sedimentary Research*, 85, 699–714. https://doi.org/10.2110/jsr.2015.39

Bussi, G., Darby, S.E., Whitehead, P.G., Jin, L., Dadson, S.J., Voepel, H.E., Vasilopoulos, G., Hackney, C.R., Hutton, C., Berchoux, T., Parsons, D.R. & Nicholas, A. (2021) Impact of dams and climate change on suspended sediment flux to the Mekong delta. *Science of the Total Environment*, 755, 142468. https://doi.org/10.1016/j.scitotenv.2020.142468

Caldwell, R.L. & Edmonds, D.A. (2014) The effects of sediment properties on deltaic processes and morphologies: a numerical modeling study. *Journal of Geophysical Research: Earth Surface*, 119, 961–982. https://doi.org/10.1002/2013JF002965

Carlson, B., Piliouras, A., Muto, T. & Kim, W. (2018) Control of basin water depth on channel morphology and autogenic timescales in deltaic systems. *Journal of Sedimentary Research*, 88, 1026–1039. https://doi.org/10.2110/jsr.2018.52

Cazanacli, D. & Smith, N.D. (1998) A study of morphology and texture of natural levees—cumberland Marshes, Saskatchewan, Canada. *Geomorphology*, 25, 43–55. https://doi.org/10.1016/S0169-555X(98)00032-4

Chadwick, A.J., Lamb, M.P. & Ganti, V. (2020) Accelerated river avulsion frequency on lowland deltas due to sea-level rise. *Proceedings of the National Academy of Sciences of the United States of America*, 117, 17584–17590. https://doi.org/10.1073/pnas.1912351117

Chadwick, A.J., Steele, S., Silvestre, J. & Lamb, M.P. (2022) Effect of sea-level change on river avulsions and stratigraphy for an experimental lowland delta. *Journal of Geophysical Research: Earth Surface*, 127, e2021JF006422. https://doi.org/10.1029/2021JF006422

Colombera, L. & Mountney, N.P. (2020) Accommodation and sediment-supply controls on clastic parasequences: a meta-analysis. *Sedimentology*, 67, 1667–1709. https://doi.org/10.1111/sed.12728

Day, J.W. & Giosan, L. (2008) Survive or subside? *Nature Geoscience*, 1, 156–157. https://doi.org/10.1038/ngeo137

Deltares. (2021a) Svn repository. https://svn.oss.deltares.nl/repos/delft3d/branches/research/Technical/20University/20of/20Delft/20190419_consolidation_compaction_v2/

Deltares. (2021b) DELFT3D-FLOW simulation of multi-dimensional hydrodynamic flows and transport phenomena, including sediments.

Dong, T.Y., Nittrouer, J.A., Carlson, B., McElroy, B., Il'icheva, E., Pavlov, M. & Ma, H. (2023) Impacts of tectonic subsidence on basin depth and delta lobe building. *Journal of Geophysical Research: Earth Surface*, 128, e2022JF006819. https://doi.org/10.1029/2022JF006819

Edmonds, D., Slingerland, R., Best, J., Parsons, D. & Smith, N. (2010) Response of river-dominated delta channel networks

20554877, 2025, 2, Downloaded from https://onlinelibrary.wiley.com/doi/10.1002/dep2.318 by Technical University Delft, Wiley Online Library on [28/04/2025]. See the Terms and Conditions (https://onlinelibrary.wiley.com/terms-and-conditions) on Wiley Online Library for rules of use; OA articles are governed by the applicable Creative Commons License

to permanent changes in river discharge. *Geophysical Research Letters*, 37, L12404. https://doi.org/10.1029/2010GL043269

Edmonds, D.A., Paola, C., Hoyal, D.C.J.D. & Sheets, B.A. (2011) Quantitative metrics that describe river deltas and their channel networks. *Journal of Geophysical Research: Earth Surface*, 116, F04022. https://doi.org/10.1029/2010JF001955

Edmonds, D.A. & Slingerland, R.L. (2010) Significant effect of sediment cohesion on delta morphology. *Nature Geoscience*, 3, 105–109. https://doi.org/10.1038/ngeo730

Edmonds, D.A. & Slingerland, R.L. (2008) Stability of delta distributary networks and their bifurcations. *Water Resources Research*, 44, W09426. https://doi.org/10.1029/2008WR006992

Edmonds, D.A. & Slingerland, R.L. (2007) Mechanics of river mouth bar formation: implications for the morphodynamics of delta distributary networks. *Journal of Geophysical Research: Earth Surface*, 112, F02034. https://doi.org/10.1029/2006JF000574

Gebremichael, E., Sultan, M., Becker, R., El Bastawesy, M., Cherif, O. & Emil, M. (2018) Assessing land deformation and sea encroachment in the Nile Delta: a radar interferometric and inundation modeling approach. *Journal of Geophysical Research: Solid Earth*, 123, 3208–3224. https://doi.org/10.1002/2017JB015084

Geleynse, N., Storms, J.E.A., Stive, M.J.F., Jagers, H.R.A. & Walstra, D.J.R. (2010) Modeling of a mixed-load fluvio-deltaic system. *Geophysical Research Letters*, 37, L05402. https://doi.org/10.1029/2009GL042000

Geleynse, N., Storms, J.E.A., Walstra, D.-J.R., Jagers, H.R.A., Wang, Z.B. & Stive, M.J.F. (2011) Controls on river delta formation; insights from numerical modelling. *Earth and Planetary Science Letters*, 302, 217–226. https://doi.org/10.1016/j.epsl.2010.12.013

Greensmith, J.T. & Tucker, E.V. (1986) Compaction and consolidation. In: van de Plassche, O. (Ed.) *Sea-level research: a manual for the collection and evaluation of data*. Netherlands, Dordrecht: Springer, pp. 591–603. https://doi.org/10.1007/978-94-009-4215-8_22

Hariharan, J., Passalacqua, P., Xu, Z., Michael, H.A., Steel, E., Chadwick, A., Paola, C. & Moodie, A.J. (2022) Modeling the dynamic response of river deltas to sea-level rise acceleration. *Journal of Geophysical Research: Earth Surface*, 127, e2022JF006762. https://doi.org/10.1029/2022JF006762

Higgins, S.A., Overeem, I., Steckler, M.S., Syvitski, J.P.M., Seeber, L. & Akhter, S.H. (2014) InSAR measurements of compaction and subsidence in the Ganges-Brahmaputra Delta, Bangladesh. *Journal of Geophysical Research: Earth Surface*, 119, 1768–1781. https://doi.org/10.1002/2014JF003117

Hillen, M.M., Geleynse, N., Storms, J.E.A., Walstra, D.J.R. & Groenenberg, R.M. (2014) Morphodynamic modelling of wave reworking of an alluvial delta and application of results in the standard reservoir modelling workflow. In: *From depositional systems to sedimentary successions on the Norwegian continental margin*. Ghent: John Wiley & Sons, Ltd, pp. 167–185. https://doi.org/10.1002/9781118920435.ch8

Jerolmack, D.J. (2009) Conceptual framework for assessing the response of delta channel networks to Holocene sea level rise. *Quaternary Science Reviews*, 28, 1786–1800. https://doi.org/10.1016/j.quascirev.2009.02.015

Jervey, M.T. (1988) Quantitative geological modeling of siliciclastic rock sequences and their seismic expression. *SEPM*, 42, 47–69.

Kaliakin, V.N. (2017) *Soil mechanics: calculations, principles, and methods*. Oxford: Butterworth-Heinemann.

Koss, J.E., Ethridge, F.G. & Schumm, S.A. (1994) An experimental study of the effects of base-level change on fluvial, coastal plain and shelf systems. *Journal of Sedimentary Research*, 64, 90–98. https://doi.org/10.1306/D4267F64-2B26-11D7-8648000102C1865D

Kozlowski, T.T. (1999) Soil Compaction and Growth of Woody Plants. *Scandinavian Journal of Forest Research*, 14, 596–619. https://doi.org/10.1080/02827589908540825

Li, L., Storms, J.E.A. & Walstra, D.J.R. (2018) On the upscaling of process-based models in deltaic applications. *Geomorphology*, 304, 201–213. https://doi.org/10.1016/j.geomorph.2017.10.015

Liu, Y., Huang, H., Liu, Y. & Bi, H. (2016) Linking land subsidence over the Yellow River delta, China, to hydrocarbon exploitation using multi-temporal InSAR. *Natural Hazards*, 84, 271–291. https://doi.org/10.1007/s11069-016-2427-5

Merckelbach, L.M. & Kranenburg, C. (2004) Determining effective stress and permeability equations for soft mud from simple laboratory experiments. *Géotechnique*, 54, 581–591. https://doi.org/10.1680/geot.2004.54.9.581

Mesri, G. (2003) *Primary Compression and Secondary Compression*. Cambridge, MA: Geotechnical Special Publication. https://doi.org/10.1061/40659(2003)5

Mesri, G. & Castro, A. (1987) Cα/Cc Concept and K0 During Secondary Compression. *Journal of Geotechnical Engineering*, 113, 230–247. https://doi.org/10.1061/(ASCE)0733-9410(1987)113:3(230)

Minderhoud, P.S.J., Erkens, G., Pham, V.H., Bui, V.T., Erban, L., Kooi, H. & Stouthamer, E. (2017) Impacts of 25 years of groundwater extraction on subsidence in the Mekong delta, Vietnam. *Enviromental Reasearch Letters*, 12, 064006. https://doi.org/10.1088/1748-9326/aa7146

Muto, T. & Steel, R.J. (2001) Autostepping during the transgressive growth of deltas: results from flume experiments. *Geology*, 29, 771–774. https://doi.org/10.1130/0091-7613(2001)029<0771:ADTTGO>2.0.CO;2

Muto, T. & Steel, R.J. (2000) The accommodation concept in sequence stratigraphy: some dimensional problems and possible redefinition. *Sedimentary Geology*, 130, 1–10. https://doi.org/10.1016/S0037-0738(99)00107-4

Muto, T. & Steel, R.J. (1997) Principles of regression and transgression; the nature of the interplay between accommodation and sediment supply. *Journal of Sedimentary Research*, 67, 994–1000. https://doi.org/10.1306/D42686A8-2B26-11D7-864800102C1865D

Nardin, W. & Fagherazzi, S. (2012) The effect of wind waves on the development of river mouth bars. *Geophysical Research Letters*, 39, L12607. https://doi.org/10.1029/2012GL051788

Nardin, W., Mariotti, G., Edmonds, D.A., Guercio, R. & Fagherazzi, S. (2013) Growth of river mouth bars in sheltered bays in the presence of frontal waves. *Journal of Geophysical Research: Earth Surface*, 118, 872–886. https://doi.org/10.1002/jgrf.20057

Nienhuis, J.H., Törnqvist, T.E. & Esposito, C.R. (2018) Crevasse splays versus avulsions: a recipe for land building with levee breaches. *Geophysical Research Letters*, 45, 4058–4067. https://doi.org/10.1029/2018GL077933

Overeem, I., Nienhuis, J.H. & Piliouras, A. (2022) Ice-dominated Arctic deltas. *Nature Reviews Earth and Environment*, 3, 225–240. https://doi.org/10.1038/s43017-022-00268-x

20554877, 2025, 2, Downloaded from https://onlinelibrary.wiley.com/doi/10.1002/dep2.318 by Technical University Delft, Wiley Online Library on [28/04/2025]. See the Terms and Conditions (https://onlinelibrary.wiley.com/terms-and-conditions) on Wiley Online Library for rules of use; OA articles are governed by the applicable Creative Commons License

Overeem, I., Hudson, B.D., Syvitski, J.P.M., Mikkelsen, A.B., Hasholt, B., van den Broeke, M.R., Noël, B.P.Y. & Morlighem, M. (2017) Substantial export of suspended sediment to the global oceans from glacial erosion in Greenland. *Nature Geoscience*, 10, 859–863. https://doi.org/10.1038/ngeo3046

Porcile, G., Bolla Pittaluga, M., Frascati, A. & Sequeiros, O.E. (2023) Modelling the air-sea-land interactions responsible for the direct trigger of turbidity currents by tropical cyclones. *Applied Ocean Research*, 137, 103602. https://doi.org/10.1016/j.apor.2023.103602

Posamentier, H.W., Jervey, M.T. & Vail, P.R. (1988) Eustatic controls on clastic deposition I—Conceptual framework. In: Wilgus, C.K., Hastings, B.S., Posamentier, H., Wagoner, J.V., Ross, C.A. & Kendall, C.G.S.C. (Eds.) *Sea-level changes: an integrated approach*. Tulsa, OK: SEPM Society for Sedimentary Geology. https://doi.org/10.2110/pec.88.01.0109

Revil, A., Grauls, D. & Brévart, O. (2002) Mechanical compaction of sand/clay mixtures. *Journal of Geophysical Research: Solid Earth*, 107, ECV 11-1–ECV 11-15. https://doi.org/10.1029/2001JB000318

Saleh, M. & Becker, M. (2018) New estimation of Nile Delta subsidence rates from InSAR and GPS analysis. *Environmental Earth Sciences*, 78, 6. https://doi.org/10.1007/s12665-018-8001-6

Stanley, D.J. (1990) Recent subsidence and northeast tilting of the Nile delta, Egypt. *Marine Geology*, 94, 147–154. https://doi.org/10.1016/0025-3227(90)90108-V

Steckler, M.S., Oryan, B., Wilson, C.A., Grall, C., Nooner, S.L., Mondal, D.R., Akhter, S.H., DeWolf, S. & Goodbred, S.L. (2022) Synthesis of the distribution of subsidence of the lower Ganges-Brahmaputra Delta, Bangladesh. *Earth-Science Reviews*, 224, 103887. https://doi.org/10.1016/j.earscirev.2021.103887

Storms, J.E.A., Stive, M.J.F., Roelvink, D.(J.)A. & Walstra, D.J. (2007) Initial morphologic and stratigraphic delta evolution related to buoyant river plumes, in: coastal Sediments '07, pp. 736–748. https://doi.org/10.1061/40926(239)56

Syvitski, J., Anthony, E., Saito, Y., Zăinescu, F., Day, J., Bhattacharya, J.P. & Giosan, L. (2022) Large deltas, small deltas: toward a more rigorous understanding of coastal marine deltas. *Global and Planetary Change*, 218, 103958. https://doi.org/10.1016/j.gloplacha.2022.103958

Syvitski, J.P.M., Kettner, A.J., Overeem, I., Hutton, E.W.H., Hannon, M.T., Brakenridge, G.R., Day, J., Vörösmarty, C., Saito, Y., Giosan, L. & Nicholls, R.J. (2009) Sinking deltas due to human activities. *Nature Geoscience*, 2, 681–686. https://doi.org/10.1038/ngeo629

Syvitski, J.P.M. & Saito, Y. (2007) Morphodynamics of deltas under the influence of humans. *Global and Planetary Change*, 57, 261–282. https://doi.org/10.1016/j.gloplacha.2006.12.001

Taylor, D.W. & Merchant, W. (1940) A theory of clay consolidation accounting for secondary compression. *Journal of Mathematics and Physics*, 19, 167–185. https://doi.org/10.1002/sapm1940191167

von Terzaghi, K. (1923) Die Berechnung der Durlassigkeitsziffer des tones aus dem Verlauf der hydronamischen Spannungserscheinungen. *Mathematischnaturwissenschaftliche Klasse, Part IIa*, 132(3–4), 125–138.

Valencia, A.A., Storms, J.E.A., Walstra, D.-J.R., van der Vegt, H. & Jagers, H.R.A. (2023) The impact of clastic syn-sedimentary compaction on fluvial-dominated delta morphodynamics. *The Depositional Record*, 9, 233–252. https://doi.org/10.1002/dep2.219

van Asselen, S., Stouthamer, E. & van Asch, T.W.J. (2009) Effects of peat compaction on delta evolution: a review on processes, responses, measuring and modeling. *Earth-Science Reviews*, 92, 35–51. https://doi.org/10.1016/j.earscirev.2008.11.001

van der Vegt, H., Storms, J.E.A., Walstra, D.J.R. & Howes, N.C. (2016) Can bed load transport drive varying depositional behaviour in river delta environments? *Sedimentary Geology*, 345, 19–32. https://doi.org/10.1016/j.sedgeo.2016.08.009

van der Vegt, H., Storms, J.E.A., Walstra, D.-J.R., Nordahl, K., Howes, N.C. & Martinius, A.W. (2020) Grain size fractionation by process-driven sorting in sandy to muddy deltas. *The Depositional Record*, 6, 217–235. https://doi.org/10.1002/dep2.85

Wake, L.M., Lecavalier, B.S. & Bevis, M. (2016) Glacial isostatic adjustment (GIA) in Greenland: a review. *Current Climate Change Reports*, 2, 101–111. https://doi.org/10.1007/s40641-016-0040-z

Winterwerp, J.C., van Kesteren, W.G.M., van Prooijen, B. & Jacobs, W. (2012) A conceptual framework for shear flow-induced erosion of soft cohesive sediment beds. *Journal of Geophysical Research: Oceans*, 117, C10020. https://doi.org/10.1029/2012JC008072

Xotta, R., Zoccarato, C., Minderhoud, P.S.J. & Teatini, P. (2022) Modeling the role of compaction in the three-dimensional evolution of depositional environments. *Journal of Geophysical Research: Earth Surface*, 127, e2022JF006590. https://doi.org/10.1029/2022JF006590

Zheng, S., Edmonds, D.A., Wu, B. & Han, S. (2019) Backwater controls on the evolution and avulsion of the Qingshuigou channel on the Yellow River Delta. *Geomorphology*, 333, 137–151. https://doi.org/10.1016/j.geomorph.2019.02.032

Zhou, Z., Wegen, M.v.d., Jagers, B. & Coco, G. (2016) Modelling the role of self-weight consolidation on the morphodynamics of accretional mudflats. *Environmental Modelling & Software*, 76, 167–181. https://doi.org/10.1016/j.envsoft.2015.11.002

Zoccarato, C., Minderhoud, P.S.J. & Teatini, P. (2018) The role of sedimentation and natural compaction in a prograding delta: insights from the mega Mekong delta, Vietnam. *Scientific Reports*, 8, 11437. https://doi.org/10.1038/s41598-018-29734-7

SUPPORTING INFORMATION

Additional supporting information can be found online in the Supporting Information section at the end of this article.

How to cite this article: Valencia, A.A., Storms, J.E.A., Jagers, H.R.A. & van der Vegt, H. (2025) The influence of syn-depositional compaction on clastic sediment distribution in river-dominated deltas: A modelling study. *The Depositional Record*, 11, 565–582. Available from: https://doi.org/10.1002/dep2.318

20554877, 2025, 2, Downloaded from https://onlinelibrary.wiley.com/doi/10.1002/dep2.318 by Technical University Delft, Wiley Online Library on [28/04/2025]. See the Terms and Conditions (https://onlinelibrary.wiley.com/terms-and-conditions) on Wiley Online Library for rules of use; OA articles are governed by the applicable Creative Commons License